 doi:10.20944/preprints202205.0072.v1

Type of the Paper (Article, Review, Communication, etc.)

Monitoring and visualization of crystallization processes using Electrical Resistance Tomography: $CaCO_3$ and Sucrose crystallization case studies

Guruprasad Rao [1], Soheil Aghajanian [2], Yuchong Zhang [3], Lidia Jackowska Strumillo [1], Tuomas Koiranen [2], and Morten Fjeld [3]

[1] Institute of Applied Computer Sciences, Lodz University of Technology, 90-924 Lodz; guruprasad.rao@dokt.p.lodz.pl
[2] LUT University, School of Engineering Science, Yliopistonkatu 34, 53850 Lappeenranta, Finland; Soheil.Aghajanian@lut.fi; Tuomas.Koiranen@lut.fi
[3] Department of Computer Science and Engineering, Chalmers University of Technology; yuchong@chalmers.se; fjeld@chalmers.se
* Correspondence: lidia.jackowska-strumillo@p.lodz.pl; Tel.: +48 699913064

Abstract: In the current research work, electrical resistance tomography (ERT) was employed for crystallization process monitoring and visualization. A first-of-its-kind MATLAB-based interactive GUI application "ERT-Vis" is presented. Two case studies involving varied crystallization methods were undertaken. The experiments involving calcium carbonate reactive (precipitative) crystallization for the high conductivity solution-solute media and the cooling crystallization for sucrose crystallization representing the lower conductivity solution-solute combination were designed and performed. The software successfully provided key insights regarding the process progress in both crystallization systems. It could detect and separate the crystal agglomerations in the low as well as high conductivity solutions using visual analytics tools provided. The performance and utility of the software were studied using a software evaluation case study involving domain experts. Participant feedback indicated that ERT-Vis software helps in reconstructing images instantaneously, interactively visualizing, and evaluating the output of the crystallization process monitoring data.

Keywords: Electrical Resistance Tomography; Visualization; Crystallization process monitoring; process operation

1. Introduction

Crystallization is a key process and is extensively used in many pharmaceutical product manufacturing and chemical applications. The process monitoring and control of the crystallization techniques in the industry have been the interest of study for many years [1]. There are primarily four types of crystallization methods: cooling crystallization, evaporative crystallization, anti-solvent based crystallization and precipitative crystallization [2]. These different types of crystallization processes have various physical principles which are used as purification and separation.

Due to the underlying physical and chemical differences and challenges, various instrumentation has been employed to monitor the course of the crystallization processes [3,4]. Collectively, crystallization monitoring and particle characterization techniques are called as process analytical technology (PAT) [5,6]. A wide range of PAT-based monitoring and feedback control approaches have been studied in recent years [7,8]. Some of the major control parameters in the crystallization monitoring are the yield which is determined by continuous monitoring of the solute concentration and crystal size distribution (CSD) [9]. Several PAT methodologies have been employed in the detection of CSD and solute concentration on laboratory scale as well as on industrial scale such as CCD cam-

 doi:10.20944/preprints202205.0072.v1

eras, hot stage microscopy, UV spectroscopy, visible light spectroscopy, Raman spectroscopy, IR and near IR spectroscopy [10–12]. These PAT tools help in crystal morphology assessments, observation of suspensions, particle size measurements, and observation of polymorphic transformations. Point based measurements such as impedance spectroscopy (IS), temperature, and pH values have been utilized to monitor the evolution of the crystallization processes and provide useful information regarding kinetics of the reactions and status of process [13,14]. IS provides a one dimensional (1-D) assessment. Multiple ultrasound based techniques have also been implemented to induce and measure crystallization progress such as single emission acoustic emissions [15] as well as ultrasound spectroscopy [16]. Sonocrystallization techniques have been extensively studied by [17] to utilize ultrasonic waves to generate cavitation in the solution to enhance micro-mixing leading to an increase in mass transfer rates and nucleation as well as control of particle size distributions. These monitoring techniques significantly improve the design of the unit operation and positively impacts the quality and yield of the final crystal products.

Among the PAT tools, tomographic sensors have the potential to provide information using reconstructed images [18]. In particular, Electrical Resistance Tomography (ERT) is an inexpensive, fast, and non-destructive modality for evaluating the crystallization processes. Fast tomographic imaging techniques are finding important applications in industrial process control [18]. The tomographic techniques using hard field imaging and soft field imaging have been studied for the purpose of crystallization monitoring. The hard field tomographic imaging uses ionizing radiation and soft field tomographic imaging involves non-ionizing radiation. The hard field imaging techniques such as Xray micro tomography, and X-ray diffraction tomography have also been utilized to study micro particulates and crystallization processes [19,20]. The soft field tomographic imaging such as ultrasound computed tomography (USCT) [21] and Electrical capacitance tomography ECT [22] have been widely reported to monitor crystallization progress in detail. In the chemical process involving large reactors and batch processes, it is of significant importance that the reconstructed image provides quantitative and accurate visualizations of highest resolution possible of the process to implement the control strategy in the reaction which can lead to precise intervention. The ERT, which is a non-destructive process tool is capable of providing higher resolutions for wide range of conductivities.

The growing industrial demand for the reactive type crystallization (also known as precipitation) is primarily due to the increasing demand for process intensification, yield efficiency enhancements, and lower energy consumption requirements [23]. In reactive crystallization, the instantaneous reactions cause differences in the density gradient within the reactor. The resultant solid product causes local variations in the conductivity distributions, which are detected using the ERT modality. In reactive crystallization processes, the main driving force of the process is a fast chemical reaction [24]. Due to the chemical reaction, the crystal nucleation and growth phenomena are very fast, requiring an immediate response from a process monitoring system [23]. In comparison, cooling crystallization evolution is relatively slower. Hence the ERT frame rate of acquisition required to capture the reactive crystallization becomes higher.

Although the one dimensional measurements such as IS, temperature and pH provide useful information, tomographic methods provide a better visual perspective of the processes in the real time environment. The 2D as well as 3D tomographic method significantly contribute in determining topology and phase as well as density distributions. They provide an opportunity to the process engineer to observe the homogeneity degree and particulate suspension distribution inside the batch reactor. As a complementary technique, tomography can provide very useful information regarding qualitative determination of the spatial distribution, a quality assurance and monitoring tool , as well as in fault detection [25–27]. The complementary utilization of the single point or 1D measurement technologies and tomographic imaging technologies can achieve better control of the crystallization process.

 doi:10.20944/preprints202205.0072.v1

It is important to evaluate and estimate the final yield along with the process progress. As the ERT imaging modality depends on the inverse imaging methodology to reconstruct the images, there is a possibility of difference in sensitivity at different distances from the sensor within the batch reactor. Variation in the parameters for the image reconstruction or the image segmentation affects the final results determining the crystal agglomerate region of interest and the accurate yield estimation. The quantitative evaluation of the crystallization progress and the factors affecting the crystallization monitoring using the ERT has been discussed extensively in [26]. It showed that multiple factors such as sensor size, reconstruction technique, conductivity of the solution under evaluation, elements in Finite Element Model (FEM) mesh, and image processing method utilized affect the quantitative evaluation of the non-conductive regions. Similar analyses for quantitative evaluations can be performed for the crystallization with varied conductivity profiles.

The reactive crystallization has fast kinetics in a high conductive solution, while the sucrose crystallization is in comparison has slow kinetics in a low conductivity medium. The process of choosing various parameters for different conductivity media for ERT image reconstruction is repetitive and time-consuming. It is important that the results obtained to be repeatable as well as the evaluation protocol can be implemented to the solutions with different conductivity profiles. The conductivity profile of the crystallization process in turn depends on the chemical and physical properties of the reactions involved. Hence it is indispensable to implement the ERT sensor which can provide the resolution within the conductivity range of the given crystallization process. Finally, the importance of advanced visualization in modern times for the fast industrial tomographic processes to analyze the objects under consideration has increased to a significant extent [28,29]. Therefore there was a need to develop a comprehensive and easy-to-use graphical user interface (GUI) based software with the functionality of data acquisition, image reconstruction, image segmentation, and crystal agglomerate visualization.

This work aimed to demonstrate the versatility and capability of ERT to visualize the crystallization process with different conductivity profiles and physical principles. In this work, an original software application called ERT-Vis was developed using MATLAB (Release R2021) with a novel approach for crystallization process monitoring and visualization for ERT data. The applicability of the software for crystallization process monitoring was successfully tested using two experimental case studies involving reactive crystallization and sucrose cooling crystallization as well as software evaluation case study involving domain experts.

The software development and experimental works were performed within the framework of the European Union Horizon 2020 TOMOCON project (smart tomographic sensors for advanced industrial process control) [18,30]. The primary focus of the project was to study the fast tomographic methods and create a multi-sensor network to monitor , visualize and implement control for batch crystallization processes [30]. The present work is a collaborative effort from three partner universities within the TOMOCON project. The Lodz University of Technology (Poland) developed the ERT-Vis software and demonstrated the case study involving sucrose crystallization, Lappeenranta University of Technology (Finland) carried out a case study involving the precipitation of calcium carbonate, and The Chalmers University of Technology (Sweden) performed the evaluation of the ERT-Vis software with a case study involving domain experts.

2. ERT System and Methods

2.1 Process engineering workflow using ERT

The process engineering workflow for a PAT modality based on tomographic image analysis can broadly be divided into five major segments as shown in Figure 1. The factors which determine quantitative accuracy using the ERT evaluation fall under these five segments. The workflow starts from the acquisition where the selection of the number of electrodes, materials used for making an electrode, sensors shape, and frame rate

Preprints (www.preprints.org) | NOT PEER-REVIEWED | Posted: 6 May 2022 doi:10.20944/preprints202205.0072.v1

of the acquisition is determined. Any process analysis using the ERT must include the following modules in order to assess the progress quantitatively. It is important for a process engineer that the control of these module is provided separately so that the calibration and quantification can be performed systematically.

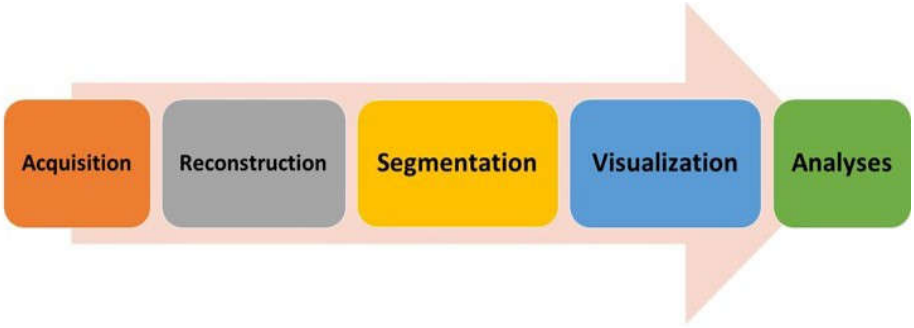

Figure 1 Process engineering ERT workflow (l. to r.): data acquisition, image reconstruction, image segmentation, 2D/3D visualization, and process analyses for control and monitoring.

2.2 General ERT system

The ERT systems consists of a complex set of sensor and data acquisition technology and inverse imaging technique to generate the image and information from the acquired voltage or current levels. It primarily is based on the Ohms law of that the material poses a resistance to the path of electric current. There are two ways in which the data acquisition takes place. These are voltage induced and current measured (VI) and current induced voltage measured (IV). Figure 2 depicts the ERT setup schematic around a reactor tank. This setup can be categorized into three modular components: data acquisition, data processing, and data visualization. The data acquisition part consists of ERT electrodes placed on the circumferential periphery of the reactor. The sensor array consists of 16 steel electrodes. These electrodes work as emitters (source) as well as receivers (sink) for the electrical signals. The cables carry the electrical signals via field programmable grid array (FPGA) boards. The FPGA boards remove any electronic noise which is received by implementing filtering algorithms as a pre-processing strategy. The data processing such as image reconstruction and image processing techniques are applied to the incoming data in real time or offline mode. The resulting images are visualized and analyzed and signals are sent back to implement the control strategy in the reactor.

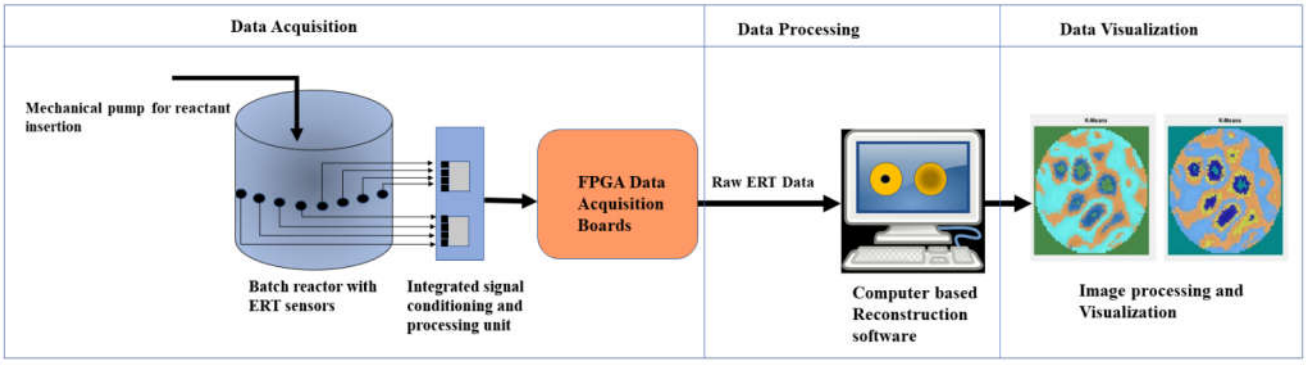

Figure 2 A schematic ERT system setup for reactive crystallization with data acquisition, data processing, and data visualization segments

2.3 Related works for ERT software development

Preprints (www.preprints.org) | NOT PEER-REVIEWED | Posted: 6 May 2022 doi:10.20944/preprints202205.0072.v1

Soft field tomography involves reconstruction based on inverse imaging. It includes various non-ionizing tomographic modalities such as ERT, ECT, USCT, microwave tomography and optical coherence tomography (OCT). Various software solutions from research labs and industry have been developed for the analysis of ERT or ECT data. A short comparison of ERT software based on the available modules for process analysis is shown in Table 1. PyEIT is open access software for ERT reconstructions [31] ; it is based on the Python programming language and offers simple 2D and 3D meshing. GREIT is software based on EIDORS for the monitoring of the thoracic region [32]. It is worth noting that GREIT is capable of reconstructing non-regular shapes, which could be beneficial in the vertical monitoring of the batch reactors or irregular shapes. The ITS Reconstruction tool suite is an ERT software development for use with ITS industrial grade ERT instruments [33]. It has multiple reconstruction algorithms for the comparison of the process data. Real-time 3D ECT was developed to obtain fast reconstructions of ECT images [34], using efficient GPU and CPU memory allocations for fast rendering of the 3D volumetric images obtained. TomoKIS studio is a software developed at Lodz University of Technology [35]. TomoKIS can be connected to multiple ERT and ECT instruments in the process tomography laboratory, so that fast and efficient rendering of 2D and 3D images can be visualized at real time. It also supports multiple reconstruction algorithms for ECT data. EIDORS is an open source extensible software package for ERT and OCT reconstruction [36–39].

Table 1. Comparison of ERT software based on the availability of different modules

Software	Acquisition	Reconstruction	Segmentation	Visualization	Researcher's Open Access
pyEIT	No	Yes	No	Limited	Yes
GREIT	No	Yes	No	Limited	Yes
ITS Reconstruction tool suite	Yes	Yes	Limited	Limited	No
Real-time 3D ECT	Limited	Yes	No	No	No
TomoKIS Studio	Yes	Yes	No	Limited	No
EIDORS	No	Yes	No	Limited	Yes
ERT-Vis	Limited	Yes (EIDORS)	Yes	Yes	Yes

3. Experimental setup and crystallization process description

The Rocsole ERT device (supplied by Rocsole Ltd., Kuopio) was utilized during the experimental works. The ERT device is voltage induced and current measured type. It was manufactured at Rocsole pvt ltd Finland. A specific type of FPGA based signal acquisition and transmission sensor unit was used to evaluate the signals in the low conductivity solutions (supplied by Rocsole technology centre, Rocsole ltd.). Sensors were mounted around the perimeter of the reactor with a diameter of 200 mm for the calcium carbonate reactive crystallization.

Two case studies were performed to test the ERT-Vis software utility. The first case involved the CaCO3 reactive precipitation crystallization experiment which involved a higher conductivity medium. The second case study was the cooling crystallization process using the super-saturated sucrose solution with a relatively lower conductivity medium. Table 2 shows the difference between certain parameters for the investigated crystallization methods. The experimental setup is explained in sections 3.1 and 3.2.

Table 2. Case studies and experimental configuration to demonstrate the application of ERT-Vis software in different crystallization processes.

Parameter	CaCO3 reactive crystallization	Sucrose cooling crystallization
Size of reactor	200 mm diameter	63 mm internal diameter
Number of electrodes	16	16

Preprints (www.preprints.org) | NOT PEER-REVIEWED | Posted: 6 May 2022 doi:10.20944/preprints202205.0072.v1

Type of reactor	polypropylene	Glass jacketed
Acquisition Frame rate	16 Hz	12 Hz
Reconstruction algorithm	Gauss-Newton	Gauss-Newton
Total Time for experiment	10 minutes	15-20 minutes
Type of crystallization	Reactive crystallization	Cooling crystallization
Stirrer speed	100 rpm	No stirrer
Input induced voltage	3 V	3 V
Range of currents detected	0-0.1 micro A	0.1-1.75 mA
Transducers frequency	156 KHz	156 KHz

3.1. Process description of CaCO3 reactive crystallization

The $CaCO_3$ reactive crystallization occurs by the addition of aqueous CO_3^{2-} into a stirred tank reactor containing a known concentration of calcium ions (calcium chloride was used as the calcium ion source). The governing chemical reaction is as follows:

$$CO_{3(aq)}^{2-} + Ca_{(aq)}^{2+} \longrightarrow CaCO_{3_{(s)}} \downarrow \quad (1)$$

The rapid liquid-phase chemical reaction results in the formation of a non-conductive solid phase in the reactor. The initial solution volume inside the reactor was 3 L as shown in Figure 3. The CO_3^{2-} reagent addition volume was 0.4 L (feed pipe diameter was 2 mm). For all the investigated cases, $CaCl_2$ (purity > 98%, Merck, Darmstadt, Germany) concentration was 1.6 g L^{-1}, mixing speed was 100 RPM (tip speed of 0.37 m s^{-1}) and the feed addition rate was 40 ml min^{-1}. The aqueous CO_3^{2-} was prepared by injecting CO_2 gas (purity > 99.9%) into sodium hydroxide (NaOH, Purity > 98%, Merck) solution—a detailed experimental procedure is provided in [40].

Experiments were performed at a temperature of (20 ±2) °C. The reactive crystallization experiments and the associated ERT-based measurements were repeated at least three times to ensure the reliability of the results.

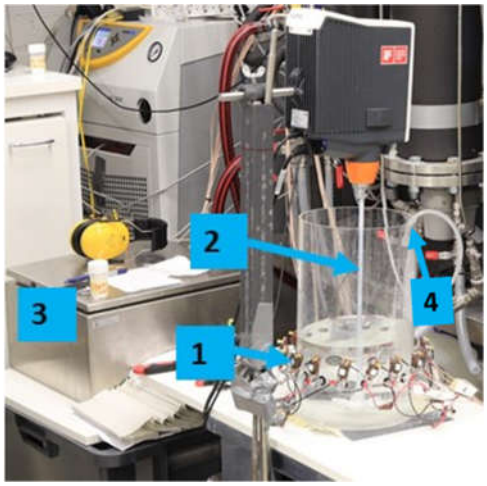

Figure 3 (1) Reactor with the ERT sensor unit mounted, (2) Rushton plastic turbine, (3) ERT device for data acquisition and process monitoring, (4) Feed pipe for the reagent addition

3.2. Process description for sucrose crystallization

Sucrose ($C_{12}H_{22}O_{11}$) crystallization using the cooling crystallization method involves the cooling of the saturated sucrose solution [41].The coefficient of supersaturation k is expressed by the ratio

$$k = \frac{\frac{Wsucrose}{Wwater}\text{in given solution at t °C}}{\frac{Wsucrose}{Wwater}\text{in the saturated solution at t °C}} \quad (2)$$

Preprints (www.preprints.org) | NOT PEER-REVIEWED | Posted: 6 May 2022 doi:10.20944/preprints202205.0072.v1

Where, Wsucrose is weight of the sucrose in the solution, Wwater is weight of the water in the solution, and t is the temperature of the solution. Experimental data on the solubility of sucrose in pure and impure solutions at various temperature has been widely reported in the literature [42,43].

Percentage of mass of soluble sucrose up to 100 °C is given as [42]

$$w_S = 64.447 + (0.08222*T) + (1.66169 *10^{-3} T^2) - (1.558 * 10^{-6} T^3) - (4.63*10^{-8}*T^4), \quad (3)$$

Where w_S is the percentage in the mass of soluble sucrose and temperature in °C is given by T. A design was proposed using the jacketed glass beaker as shown in the Figure 4 (a) to perform the cooling of the saturated sucrose solution. The jacketed beaker as the name suggests has a temperature maintaining glass jacket around the reactor. The outer height and the outer diameter of the beaker measured 195 mm and 120 mm respectively. The inner height and the inner diameter of the beaker measured 175 mm and 95 mm respectively. The challenge of using the glass reactor involves an inability to drill holes for the ERT sensor placement as in the case of reactor made from polymer material. Hence a novel design for the placement and insertion of ERT sensor unit was 3D printed as shown in Figure 4 (b). The sensor was placed within the beakers circumference. The black non-conducting paint was applied on the back side to prevent the leakage of current. The MCX coaxial connectors were utilized to connect to the Rocsole device. The coaxial cables were soldered to the sensor and a rubber insulation was provided to avoid any contact with the supersaturated solution which would result in noise in the acquisition signal.

(**a**) (**b**)

Figure 4 (a) Jacketed beaker with supersaturated sucrose solution inside the ice bath. (b) 3D printed sensor insert to mount ERT electrodes

The 3D sensor insert was designed using the software Blender version 2.79b. It was 3D printed using the Ultimaker version 3 Extended software with an accuracy of 1 mm with the help of the software Cura 4.6. The sensor insert was printed using acrylonitrile butadiene styrene (ABS) material. The jacketed beaker was filled with water at 0° C and placed in the ice bath for maintaining the constant temperature. Saturated sucrose solution weighing 400g was prepared from Polski Cukier sugar crystals and tap water. The solution was heated up to 90 °C and was poured inside the beaker and measurements were taken at reducing temperature of 90 °C, 45 °C, 40 °C and 35 °C.

4. Development of the software ERT-Vis

The Electrical Resistance Tomography (ERT) can provide 2D/3D images supporting analytic tasks within chemical process analysis. Effective use of such images relies criti-

Preprints (www.preprints.org) | NOT PEER-REVIEWED | Posted: 6 May 2022 doi:10.20944/preprints202205.0072.v1

cally on the choice of reconstruction parameters and flexibility to change them quickly. We systematically studied such parameters for analyzing the non-conductive materials in the low conducting media [26]. For cylindrical chemical batch crystallization reactors, a conventional parameterization approach relies on testing and comparing of the number of iterations, finite element model mesh structure, hyperparameter values, and tolerances with simulations and phantoms. We conjecture that interactive parameterization of segmentation methods and morphological image processing will be critical to evaluate the spatial accuracy of the reconstruction in low conductivity environments. A visual analytics-based software ERT-Vis to visualize reconstructed ERT images and apply runtime image processing techniques is presented. This software consists of four modules for ERT data analyses: acquisition, reconstruction, segmentation, and visualization. The software evaluation case study involving domain experts was also conducted.

It was imperative that there was a need to develop a software that would help address the unique requirements of the process engineer and is versatile. Such software must be able to acquire the data from ERT, reconstruct an image according to the flexible parameters chosen by the process engineer, perform the image processing tasks and provide the flexibility to visualize the data in the requisite format depending on the type of the crystallization experiment performed. The human-computer interaction was an essential part of the experiment as the requirements of the process engineer varies for different crystallization methods. The developed software was tested with the involvement of domain experts in the field of tomography. A special module on generating videos was added based on the common feedback from the domain experts.

4.1. Development of the application modules and GUI

ERT-Vis is a MATLAB-based software application created using the MATLAB app-designer toolbox. The GUI tool `'UIAxes'` was extensively used to display plots, panels, reconstructed and segmented images. A general selection header strip can be seen across all the modules of the software for interactive selection, activation of the modules, and navigating through the image frames either sequentially or to a specified frame. The START ERT-Vis push button must be pressed to initialize the ERT-Vis software from the general selection header strip before beginning to use the application to initialize the libraries.

Four modules were implemented in the prototype software in line with the workflow of the data in the ERT data acquisition and analysis system. These modules differed in their functions and were assimilated into separate tabs for better accessibility. In the current version of the ERT-Vis software, a researcher option has been added for enabling and disabling the four modules by pressing the activate push buttons in the general selection header strip. This reduces the number of computations required to update the displayed plots and images saving the time. With the "Activate acquisition" state button, the acquisition module tab is rendered functional. With the "Activate reconstruction" state button, the reconstruction capabilities of the ERT-Vis software in the reconstruction tab are switched on. With the "Activate Segmentation" state button, the image processing capabilities from the MATLAB image processing toolbox are utilized to segment and process the data. With the "Activate Visualization" state button, users have the capability to visualize the data in the various available colormaps of the extracted individual RGB channels of the image, and they can implement binarization by grey-level thresholding or flood-fill segmentation on the extracted images.

The general selection header also consists of the reconstruction status LED indicator. This LED blinks red prior to the execution of the reconstruction algorithms and turns green when the reconstruction is completed. The default status of the reconstruction LED is yellow. With the "Frame Select" slider the current frame under observations can be moved to the desired location. The range of the "Frame Select" slider value is from 0 to 900 and can easily be changed via the MATLAB App designer. Alternatively, researchers can automate the process using the variable designated to track the number of frames in the uploaded data. The spinner "Frame Step" accepts the numerical input

Preprints (www.preprints.org) | NOT PEER-REVIEWED | Posted: 6 May 2022 doi:10.20944/preprints202205.0072.v1

within the range of "Frame Select" slider values and reconstructs the user-defined frame. This feature is convenient to observe minor changes that occur within micro-seconds of the process with fast kinetics acquired using a high frame rate ERT acquisition device one frame step at a time.

4.2. Module 1 : Data Acquisition

In this tab, data can be acquired using the ERT device online over the Wi-Fi connection or visa LAN connection. The "Data Acquisition" tab can be seen in Figure 5. The "Data acquisition" module of the ERT-Vis was tested with Rocsole device at Lodz University of Technology as an independent module. At the LUT University the ERT device was connected with LAN connectivity. At the Lodz University of Technology the ERT data was obtained by forwarding it via the in-house TomoKIS Studio software [35] which was physically connected to the Rocsole device through an internet router. Rocsole Ltd. provided DLLs for enabling the connection of the ERT device to the TomoKIS studio software. The case study evaluations for cooling crystallization using the ERT-Vis were performed from the recorded data.

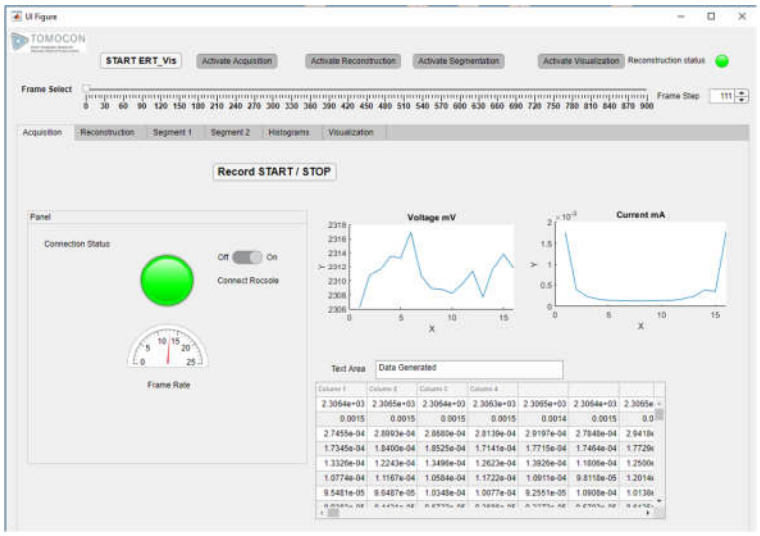

Figure 5 ERT-Vis: Data acquisition module tab at initial condition

Using the "on-off" toggle switch the user can be connected to the ERT device over Wi-Fi. The status of the ERT device connection is indicated using the LED "Connection Status" with color. The disconnection is indicated using 'red color'. The LED status indicator turns green if the PORT status is open and the device is connected. The default status before the first reconstruction is yellow. The currents acquired and the voltages of the frame are visualized in the "Currents" and "Voltages" plot. The numerical streaming data can be visualized on the table columns below the plots in the MATLAB table. The streaming data is saved into the text format using the "Record START/STOP" State button

4.3. Module 2: Reconstruction

In this module, the main task of the reconstructions from the ERT data are achieved. The images obtained after the ERT reconstruction depend on various factors such as hyperparameter values, the number of iterations, the FEM mesh model structure, the number of sensors, and the number of pixels in the resultant image. Within this module, the user has the flexibility to choose the reconstruction method and make fine adjustments to achieve better results and visualize the results immediately and interactively.

The "Reconstruction" tab is shown in Figure 6. In this version of ERT-Vis three reconstruction algorithms have been implemented: the Gauss-Newton (GN) algorithm, the

Preprints (www.preprints.org) | NOT PEER-REVIEWED | Posted: 6 May 2022 doi:10.20944/preprints202205.0072.v1

Total-Variation (TV) algorithm and the Linear Back Projection (LBP) algorithm. These algorithms have been implemented using EIDORS open-source software. EIDORS version 3.10 is central to the reconstruction module for ERT-Vis [44]. EIDORS is an open-source MATLAB toolkit for electrical resistance tomography [45]. Nonlinear or ill-posed problems in electrical resistance or electrical capacitance tomography are approached using a finite element model (FEM) for forward calculations. A regularized nonlinear solver is implemented to obtain a unique and stable inverse solution. This includes a derivation of the formula for the Jacobian matrix or the sensitivity matrix based on the complete electrode model.

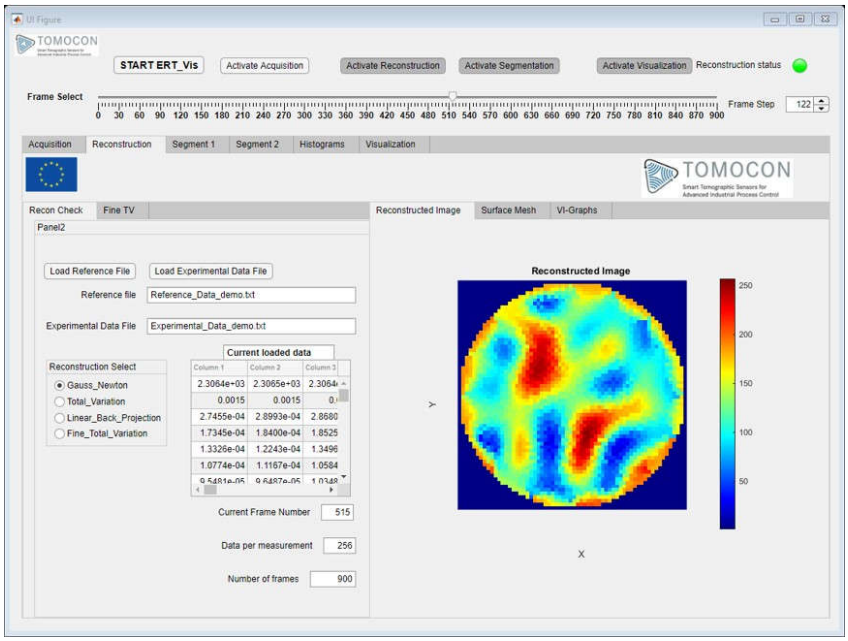

Figure 6 ERT-Vis Reconstruction module tab

The "Reconstruction" tab is vertically divided into two sections. This tab is activated after pressing the "Activate Reconstruction" state button. In the "Recon check" tab of the reconstruction module on the left, the reference data and the experimental data can be imported using the push button "Load Reference File" and "Load Experimental Data File" respectively. The file names of the imported experiment are displayed and verified in the Edit text Field box "Reference File" and "Experimental Data File" respectively. The reconstruction algorithm can be selected from the Button group "Reconstruction Select" out of the four options currently provided. The change in the selection of the "Reconstruction Select" button group results in the generation of a new image in the "Reconstructed Image" tab on the right side. The numerical edit text fields "Current Frame Number", "Data per measurement", and "Number of frames" display the current frame monitored, data points in the single frame of the measurement, and the total number of frames in the current experimental data-set. On the right-hand side section, as shown in Figure 7, the 2D reconstructed image is observed in the "Reconstructed Image" tab. This provides us with a 2D visualization. In the "Surface Mesh tab", a 3D surface mesh provides a 3D visualization. The information regarding the induced voltage stability using the average and standard deviation of the voltages in the frame can be observed numerically in the "VI-Graphs" tab. The information regarding the minimum and maximum current in the frame is also observed in this tab to check the sensor capabilities for detecting the currents in the solution provided.

Preprints (www.preprints.org) | NOT PEER-REVIEWED | Posted: 6 May 2022 doi:10.20944/preprints202205.0072.v1

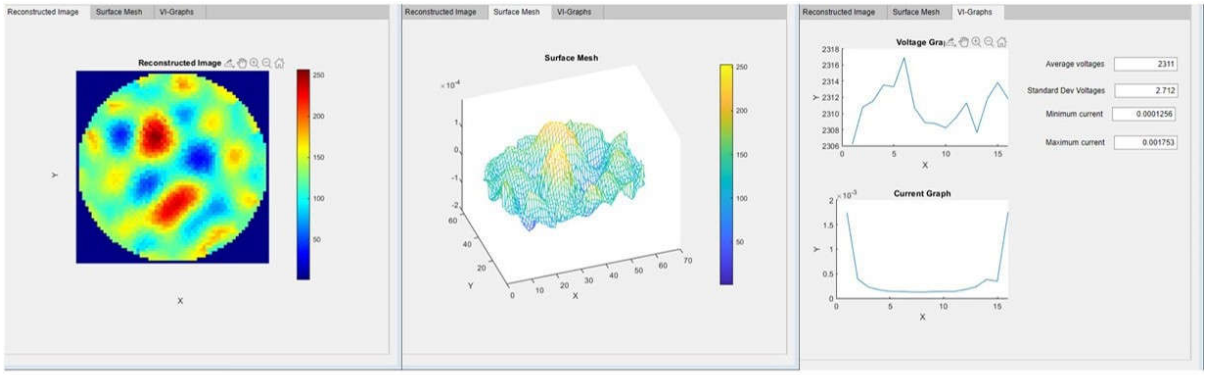

(a) **(b)** **(c)**

Figure 7 Reconstruction module: Panel for advanced visualization tabs (a) 2D reconstruction, (b) 3D surface mesh visualization, and (c)graphical and numerical observations.

Additionally, the reconstruction algorithm Total-Variation can be controlled from the "Fine TV" tab on the left axes as shown in Figure 8 (a). Here the number of iterations is varied from the spinner "Number of iterations". The Jacobian background value can be edited using the numerical Edit Field "Jacobian Background Value". The hyper-parameter value and tolerance can also be varied from 10E-5 to 10E5 with the help of the separate sliders along with the multiplication factor selected from the button group. They are color-coded blue and green for easy access. The values set are visible in the numerical edit field box "HP" and "Tol" respectively.

To observe the precipitation frame by frame as a video, two new functionalities in the ERT-Vis software were added in the reconstruction tab as shown in Figure 8 (b). They are called as “VideoGen” and “VideoSave”. Using this functionality, a user could generate a video to observe the progress of the reaction from the saved data and save the video files. This helps in fast analysis of the raw data using different reconstruction techniques and after application of the various image processing techniques. The user must put the range of frames to observe in the “From_Frame” and “To_Frame” numerical input boxes and provide the location after pressing the “Save Location” button in case the video is required for further analysis.

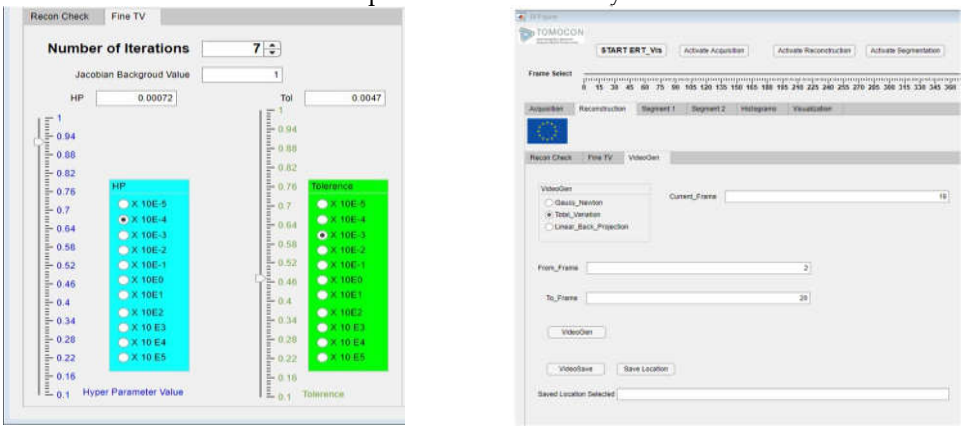

(**a**) (**b**)

Figure 8 (a) Reconstruction module: Total-variation-algorithm tab (selecting reconstruction parameter value progression from coarse to fine/detailed) (b) VideoGen function in ERT-Vis.

Preprints (www.preprints.org) | NOT PEER-REVIEWED | Posted: 6 May 2022 doi:10.20944/preprints202205.0072.v1

4.4. Module 3: Segmentation

In this module, there are two tabs for segmenting the reconstructed ERT image. In the "Segment 1" tab there are six panels as shown in Figure 9. The output of the EIDORS software provides an indexed image which is mapped on a 'jet' colormap and displayed on the "Indexed Image" panel. This indexed image is converted to the RGB true color image using the function `mat2im()` [46]. The converted true-color image is visualized in the "RGB-True Color Image" panel. The indexed image is converted into the gray image using the MATLAB inbuilt function `rgb2gray()`. This resulting image is displayed in the "Gray" panel. The OTSU segmentation is applied to this gray image using the MATLAB function `otsuthresh`() after evaluating the histogram using the function `imhist`. The resulting image is shown in the "OTSU" panel. In the "Gray-connected" panel the result from the flood-fill image segmentation performed using the function `grayconnected()` MATLAB function is displayed. This is an interactive segmentation method where the user provides input interactively. For this segmentation to operate three inputs are required: The row number, the column number and the tolerance. The row and column input for the initial seed point is to be put in the spinner "Seed Row" and "Seed Column" within the range of 0 to 64. The tolerance for the range of gray levels included can be controlled using the slider below the axis named "Tolerance" within the range of 0 to 1. In the "Local Adaptive" panel, the results from the MATLAB image segmentation function `adaptthresh()` are visualized. The threshold value for the binarization is controlled using the slider "Threshold" below the axis. In Figure 9 (a) the Segment 1 tab can be observed with six image displays showing results of various image processing algorithms. Figure 9 (b-e) show the resultant reconstructed as well as image after application of image processing algorithms.

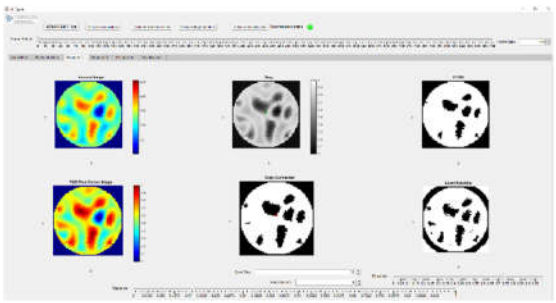

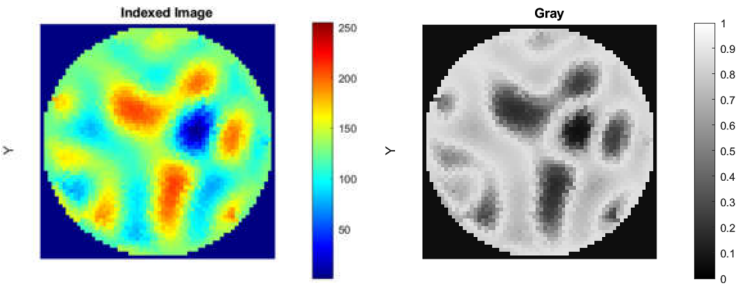

(b)

(c)

(d)

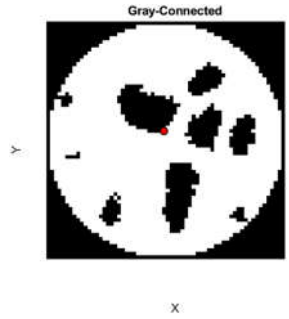

(e)

(a)

Figure 9 Segmentation module: (a) Segment 1 TAB (b) Indexed image,(c) Gray image (d) OTSU-segmented image, and (e) Gray-connected segmented image.

In the "Segment 2" tab of the segmentation module an advanced segmentation method of K-means clustering is provided. The k-means clustering in MATLAB is im-

Preprints (www.preprints.org) | NOT PEER-REVIEWED | Posted: 6 May 2022 doi:10.20944/preprints202205.0072.v1

plemented using the function `imsegkmeans`. This is an advanced segmentation technique which segments image data using unsupervised learning method. The user has the ability to interactively provide the number of segments as an input. This tab consists of three display panels as shown in Figure 10.

In the panels: The ERT reconstructed image and 16 bit unit gray image can be visualized respectively. The 16-bit gray image is obtained using the MATLAB function `im2uint16`. The Uint16 image obtained is used to implement the K-means clustering. Using the spinner "Number of Segments" the input values for classifying the image into the various clusters are provided. This provides the flexibility to classify and extract the region cluster of interest for further analysis and study. Different clusters are automatically color-coded for better visualization.

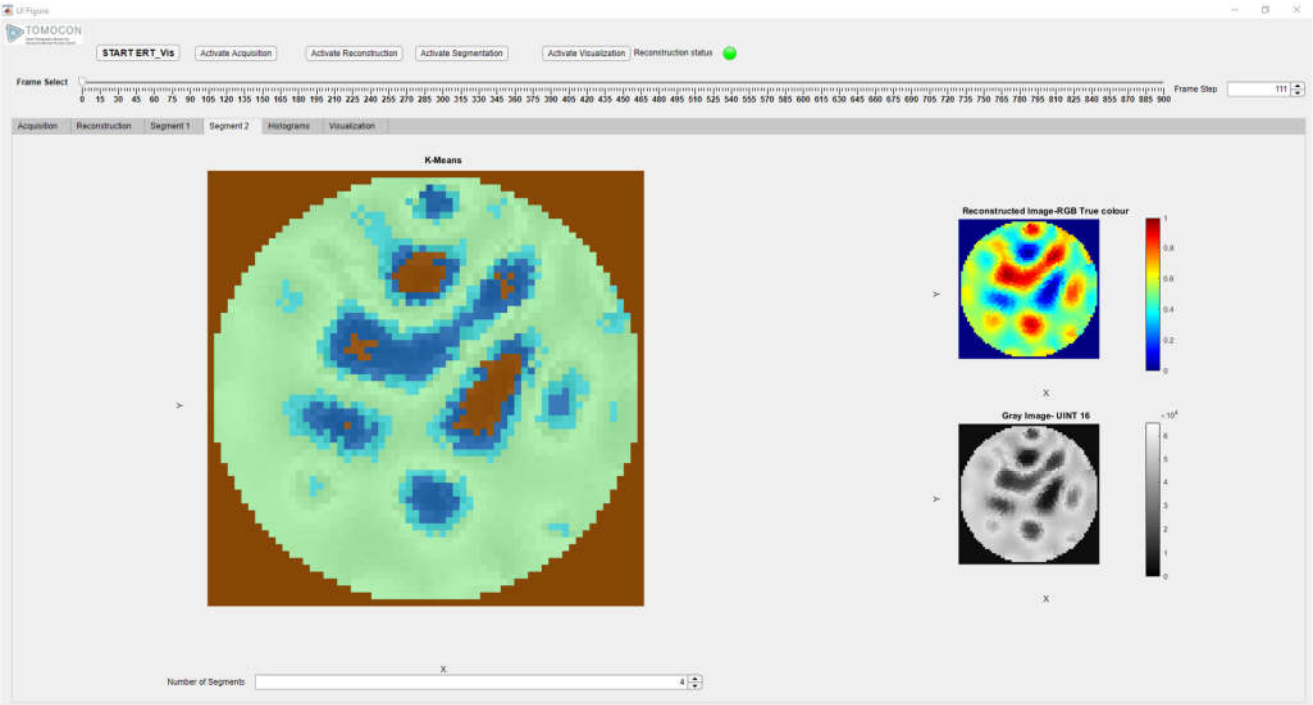

Figure 10 Segmentation module: Advanced segmentation tabs for observing the K-means clusters.

4.5. Module 4: Visualization

In the "Visualization" tab group there are seven sub-tabs as shown in Figure 11 (a). The first four tabs "RGB", "R-Channel", "G- Channel", and "B-Channel" are only visualization tabs. The next three tabs "R-Channel-binarize", "G-Channel-binarize, and "B-Channel-binarize" are for advanced interactive visualization and segmentation of the extracted image color channels. In the tab "RGB", the reconstructed image and the images from the color channels extracted are shown in four axes named "Reconstructed Image", "R-Channel Extracted Image", "G-Channel Extracted Image", and "B-Channel Extracted Image" respectively as shown in Figure 11.

Preprints (www.preprints.org) | NOT PEER-REVIEWED | Posted: 6 May 2022 doi:10.20944/preprints202205.0072.v1

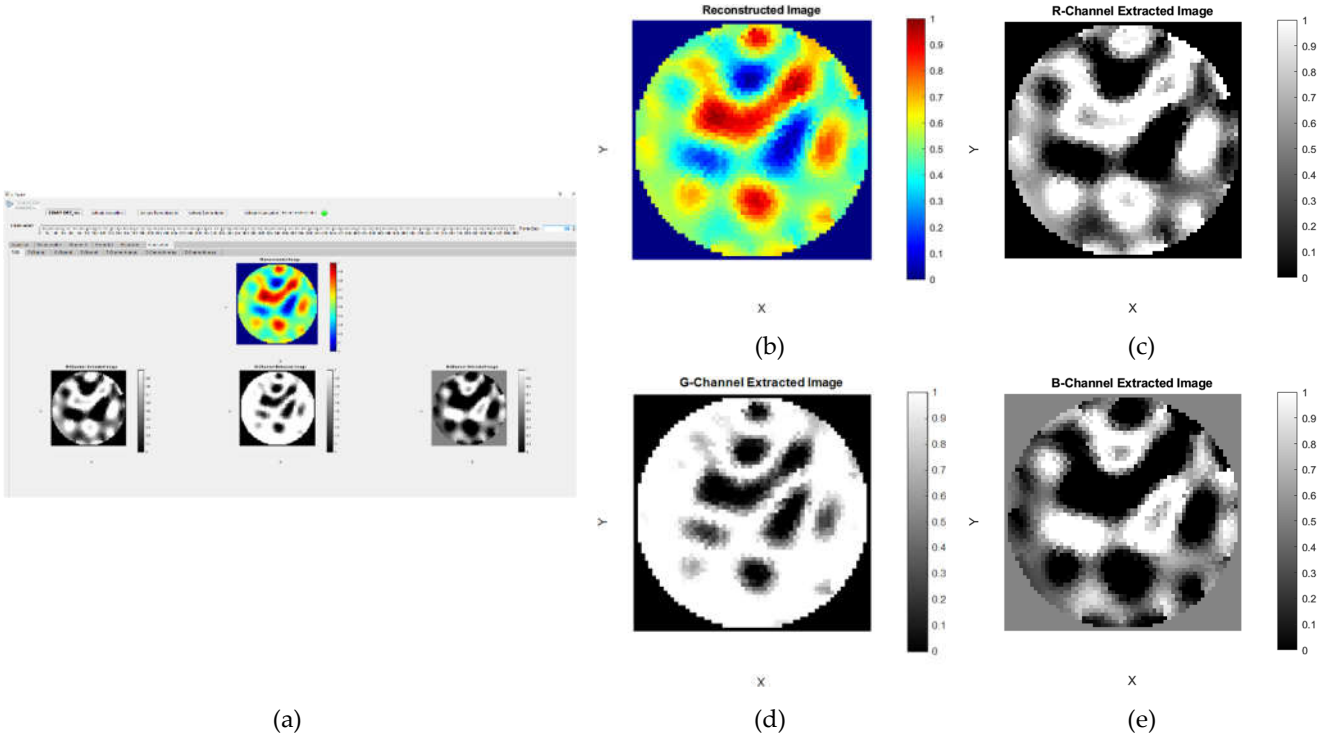

Figure 11 Visualization module: Color channel extraction and visualization tab. (a) RGB tab (b) reconstructed image (c) R-Channel image (d) G-Channel image (e) B-Channel image

The ERT reconstructed RGB true-color images were extracted into the three separate images and displayed in these panels using the MATLAB function `imsplit`. The extracted channels have been mapped to six different MATLAB colormaps such as `copper`, `hot`, `summer`, `autumn`, `winter`, and `spring` [28]. These images with six colormaps are simultaneously displayed in six panels in "R-Channel", G-Channel, and "B- Channel" tabs. The titles of panels are similar to the names of the colormaps as `"copper"`, `"hot"`, `"summer"`, `"autumn"`, `"winter"`, and `"spring"` as shown in Figure 12 (a-g).

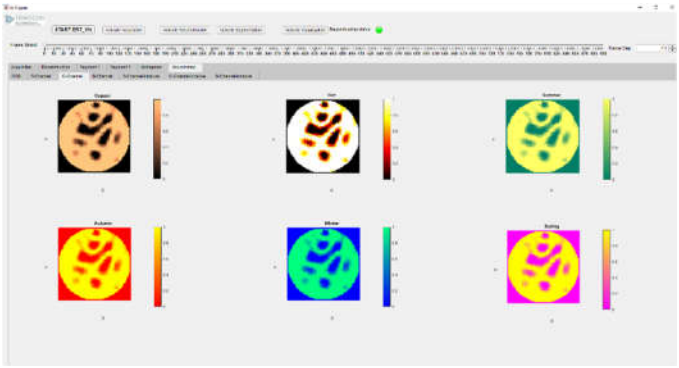

(a)

Preprints (www.preprints.org) | NOT PEER-REVIEWED | Posted: 6 May 2022 doi:10.20944/preprints202205.0072.v1

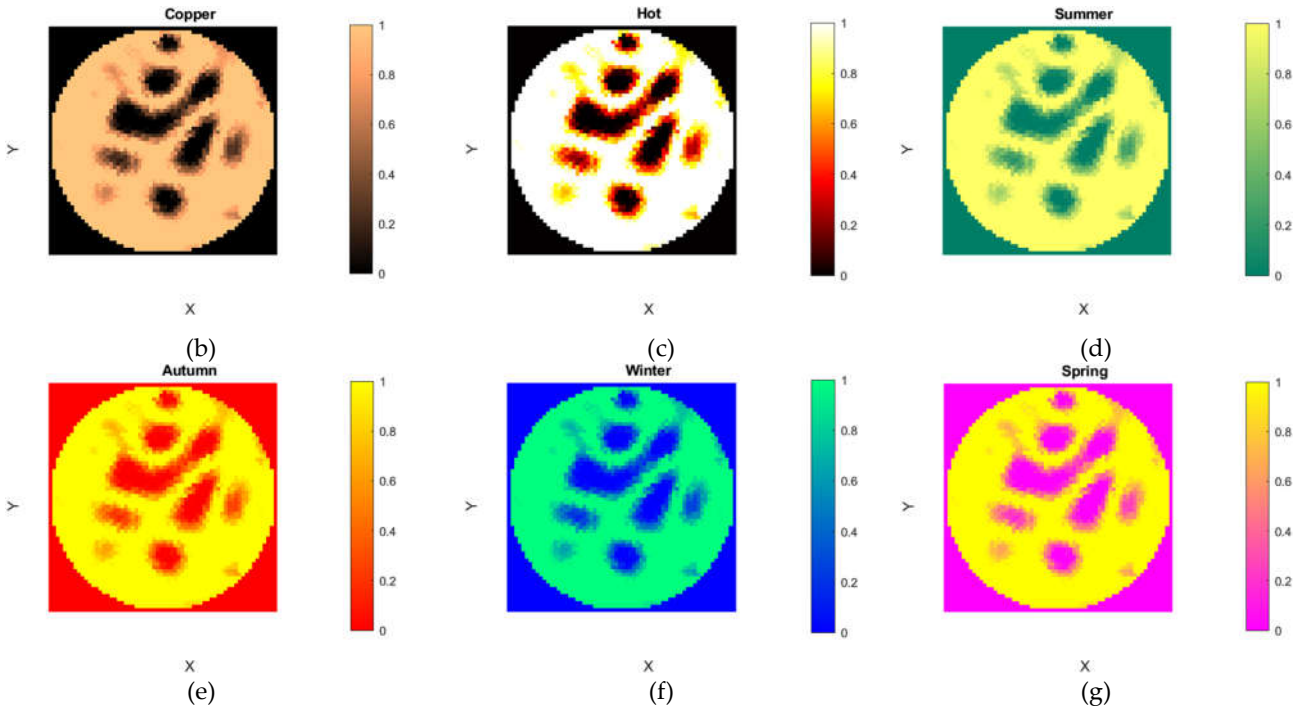

Figure 12 Visualization module: Simultaneous Colormap observations tab. (a) G-Channel observed with various colormaps, colormaps implemented (b) copper (c) hot (d) summer (e) autumn (f) winter (g) spring.

The advanced interactive visualization and segmentation tabs were designed for every extracted color channel of the image. This can be visualized for the tab "G-Channel-binarize" as shown in Figure 13. It contains four panels. "RGB Image", "Gray Scale Image", and "G-Channel Image" can be seen on the right vertical strip. The user can interactively select the colormap from the button group "G-cmap" to visualize the extracted color channel. Using the slider value from "Binarize threshold" as a threshold, the images are binarized using the MATLAB function `imbinarize()`. Using the spinners "Seed Row" and "Seed Column" along with the slider "Tolerance" as input to the MATLAB function `grayconnected()` ensures the interactive segmentation of the extracted color channel.

Preprints (www.preprints.org) | NOT PEER-REVIEWED | Posted: 6 May 2022 doi:10.20944/preprints202205.0072.v1

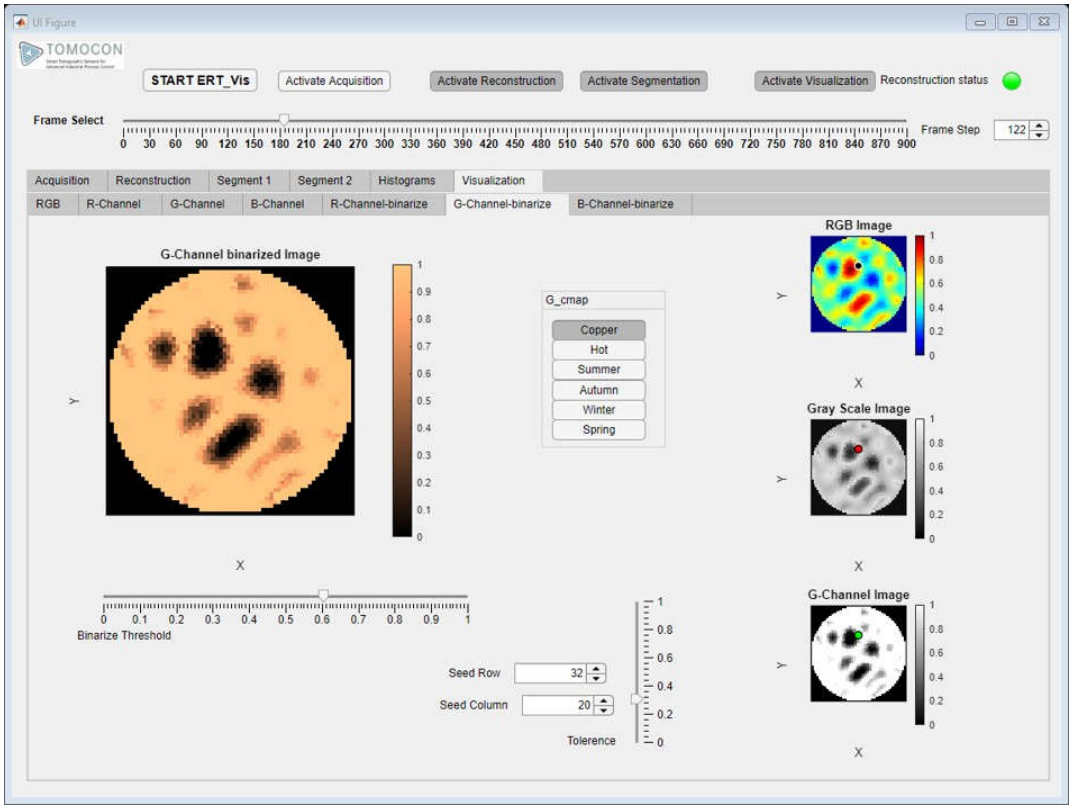

Figure 13 Visualization module: Advanced interactive visualization and segmentation tab.

5. Results

5.1 Software evaluation case study

5.1.1 Case study

We demonstrate ERT-Vis with a case study involving four domain experts performing several tasks to evaluate the effectiveness of our application. The four participants are denoted as P1, P2, P3, and P4 respectively, and their individual domain backgrounds are elaborated below. The case study was successfully organized across various countries with domain experts. The online co-ordination was achieved using the MS-Teams software from Microsoft. One issue arising during the study was the limitations of the software on Mac computers. To overcome this the domain experts were given remote access to the author's laptop to conduct the tasks.

P1: PhD student who has been working with ERT for three years.

P2: Associate professor with over 15 years of experience in ERT technology.

P3: Professor with more than 20 years of experience in tomography.

P4: PhD student with almost three years of hands-on tomographic experience.

The case study comprised three parts: a preparation meeting, separate implementation with real-time feedback from each participant, and a post-feedback session. To start, each participant attended an initial session online and consented to be recorded over the whole process. In the preparation meeting, we clarified the relevant issues and then demonstrated a tutorial of ERT-Vis for them. Next, every participant was assigned with a time slot and requested to perform an ERT visual analytics task including seven microtasks as illustrated below. Each expert received the same task list but they obtained distinct results since they were asked to select different images at the beginning (denoted with "X" in the illustration). After completion, the participants had another opportunity to provide extra post-feedback despite having given real-time comments previously.

 doi:10.20944/preprints202205.0072.v1

5.1.2 The ERT visual analytics task

Task-1: Load the reference data, then load the experimental data.

Task-2: Choose the frame number X using the slider.

Task-3: Check various image reconstructions. Check the 2D images and 3D meshes-V-I numerical data in different tabs.

Task-4: Observe the segmentation results. Switch to any other segmentation methods.

Task-5: Observe the histograms of the images.

Task-6: Observe the separated R, G, and B channels of ERT images.

Task-7: Select and change the colormaps of the extracted R, G, and B channels.

Task-8 (optional): Conduct binarization using the threshold and visualization for the gray-connected seed row/column.

The participants first checked the whole graphical user interface (GUI) of ERT-Vis, then executed the loading of the necessary data files. P1 said, "Loading files is very immediate, which is not common in the similar tools I used before." P2 complimented the GUI as it is straightforward for users to have an overview of the whole application. Next, they successfully chose a designated frame number using the slider and checked the reconstruction results and the visualizations. "It is considerably more convenient to simultaneously check both 2D and 3D visualizations in the same panel," P4 commented, because he found it useful for conducting related analyses. He then added, "Putting reconstruction as the first module is valuable for domain users to better understand the problems." Of the provided various segmentation results, both P2 and P3 hypothesized the diversity of selecting different segmentation methods for comparative analysis. P1 noted, "It's very time-saving to observe the histograms of the images as they took only a short time to be displayed". Notably, they regarded the part of observing R, G, and B channels of the ERT images as a novel feature compared to the existing similar domain software applications. Upon the completion of all the tasks, P2 affirmed that ERT-Vis possesses a consistent and coherent workflow which makes it comfortable for users to follow, and suggested that it was advisable to implement it. P3 said he was "amazed by the content contained in a single application as it supports multi-modal visual analysis." The ability of toggling different reconstruction methods, segmentation methods, and visualization categories were highlighted by every participant.

5.1.3 Insights

Time-saving: The primary characteristic reported from the participants regarding ERT-Vis was immediacy. They spotted that there are no built-in iterative algorithms to make the application display the results after changing the arguments. Different from other applications, ERT-Vis adopts the simple algorithm selection–result display' strategy, which ensures the users can simultaneously choose the desired method then obtain the corresponding result in a short time. Based on the quick response time throughout the applications, the efficacy and efficiency of tasks are remarkably improved.

Descriptive: The participants pointed the descriptive information included in ERT-Vis. Most of them indicated that ERT-Vis offers parallel analysis of data acquisition, reconstruction, segmentation, and visualization, which is a significant breakthrough in comparison to other tomography-related visual analytic tools they had used before. The specific enrichment of each module was appreciated as there are multiple approaches supplied in every module. For example, the users have the capability to choose diverse reconstruction and segmentation methods when carrying out the hands-on analyses. The workflow was well designed so as to support comprehensive visual analysis for ERT-related decision-making. In particular, P1 noted that he was astounded by the 'seed segmentation' part as it facilitates the users to have a deeper understanding of the domain problems.

User-friendly: Overall, ERT-Vis was deemed a user-friendly application by the participants. They reported that the design of the GUI is intuitive and comprehensible, and agreed that ERT-Vis is easy to use throughout the whole operation period. The concise-

Preprints (www.preprints.org) | NOT PEER-REVIEWED | Posted: 6 May 2022 doi:10.20944/preprints202205.0072.v1

ness and transparency of the interface gave them a clear overview of each module, enabling them to easily grasp the functionality to proceed with their work. In particular P4 was especially satisfied with the layout of ERT-Vis as it shows several outputted image side by side in the same interface. He felt it is straightforward and convenient to compare the results under such settings.

Limitations: Certain limitations regarding ERT-Vis were pointed out by the domain experts. One common request was the facility of generating the videos from the entire frames and the possibility to save images. More specifically, P3 indicated that the VI-graph should be designed to a tunable panel, which would allow users to better interact with the visualization results. P4 requested for inclusion a time-stamp over the reconstructed image tab for comparison with future imaging modalities. As the frame rates are higher the visibility of microseconds would inform the user of the status of the crystallization within the time differences of microseconds. Prior smoothness selection has not been included yet. The 3D reconstruction modules and algorithms have not yet been implemented and will be incorporated in future iterations.

5.2. Results for CaCO3 precipitative crystallization using ERT-Vis

Initially, a metallic impeller was utilized in the experimental setup. The reconstructions with the metallic impeller included significant noise during the acquisition of the ERT signals. Therefore, a plastic-made Rushton impeller was utilized for agitation. Using the ERT-Vis software, the detection and resolution of the issue of the noise in the reconstructed images were resolved swiftly, which optimized the overall time required for the experimentation. Quick analysis prior to the start of experiments provided us with an added advantage in performing closed-loop control experiments [27].

Figure 14 shows Reconstructed images of plastic, metal and both plastic and metal together along with the surface mesh .The images were reconstructed using the one-step Gauss-Newton reconstruction method. The difference between the metal and the plastic stirrer is detected. The metallic stirrer included noise in the ERT single electrode acquisition as well as reconstructions. Hence plastic stirrer was utilized. As a process engineer, this was important information that helped in avoiding the noise generated using the metallic stirrer when the stirrer was switched ON.

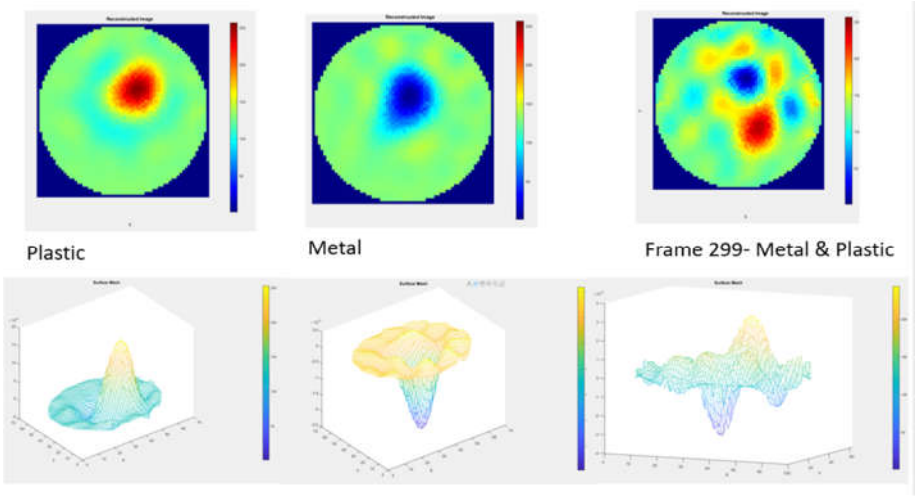

Figure 14 Reconstructed images of plastic, metal and both plastic and metal together along with the surface mesh

Preprints (www.preprints.org) | NOT PEER-REVIEWED | Posted: 6 May 2022 doi:10.20944/preprints202205.0072.v1

The evaluation for the changes in the electrical currents due to the changes in the concentration of the calcium chloride in the solution was tested. Figure 15 shows the changes in the average electrical current from 0 gL^{-1} to 66.7 gL^{-1}. It was noted that the current changed from 0.02 μA until 0.1 μA. These tests proved that the FPGA signal conditioning units of ERT device was capable of resolving minor conductivity changes in a highly conductive solutions involving calcium chloride.

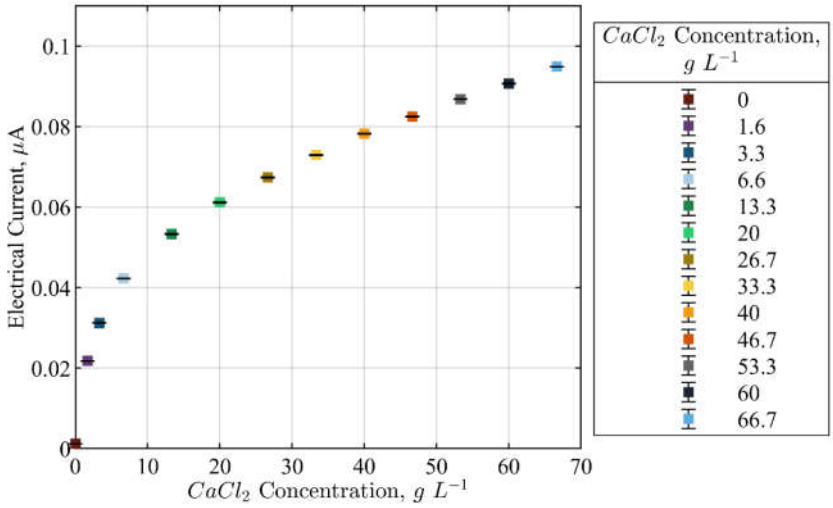

Figure 15 Average electrical current measurements evaluated for 100 frames for different concentrations of $CaCl_2$ solutions with no stirrer motion.

Further tests using ERT-Vis software were conducted to evaluate the detection of calcium carbonate CaCO3 inside the reactor. For this purpose VideoGen tool was used and the images were saved. The images prior to the addition of any crystal additives consisted of noise due to motion of water and amplification of minor differences by the Gauss-Newton reconstruction algorithm as shown in Figure 16 (a). Powdered calcium carbonate weighing 100g (VWR, purity>99%) was put inside the reactor and the images were reconstructed using Gauss-Newton algorithm. The changes in the reactor were visible and the color of the reactor turned opaque. The solid micro particles of calcium carbonate appeared as a non-conducting region as shown in the Figure 16 (b).

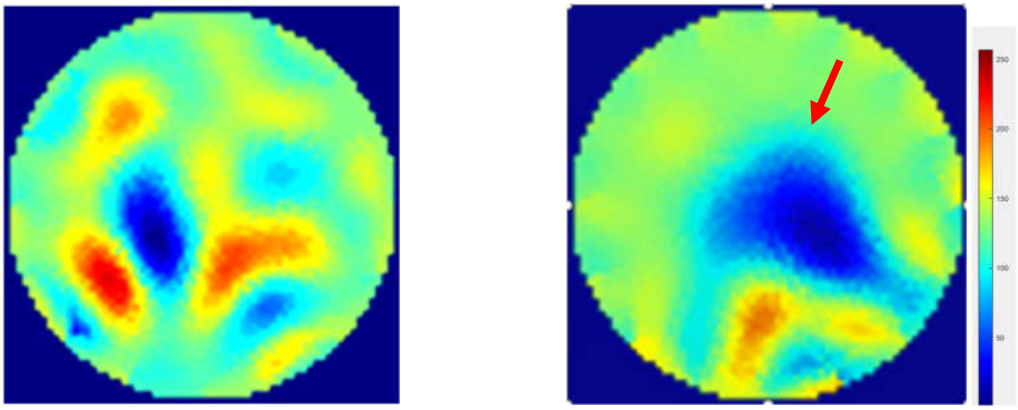

(a) Water inside reactor (b) CaCO3 insertion(blue)

Figure 16 (a) Water with ripples (b) Detection of $CaCO_3$ particles in water

Preprints (www.preprints.org) | NOT PEER-REVIEWED | Posted: 6 May 2022 doi:10.20944/preprints202205.0072.v1

Final tests were done using the ERT-Vis software to detect the presence of the calcium carbonate in the base solution of NaOH and calcium chloride to detect the presence of calcium carbonate crystals. Figure 17 shows the ERT reconstructed images for the observation of the settling of the $CaCO_3$ within the reactor. The calcium carbonate $CaCO_3$ particles can be observed in the color red. As the time progresses, we can see that the precipitation bolus is moving downwards in the reactor.

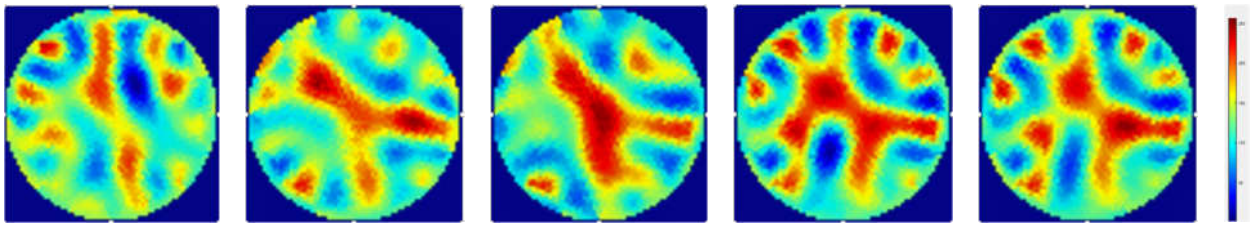

Frame 6000 Frame 6040 Frame 6080 Frame 7000 Frame 7080

Figure 17 Observation of settling of $CaCO_3$ in the suspension at various stages of experiment. Red regions indicate the $CaCO_3$ crystal regions

To determine the calcium carbonate presence in the solution using the unsupervised learning method K-means clustering segmentation was implemented. Figure 18 (a-d) shows the effect of changing the number of clusters in the image to two, three, four, and five clusters.

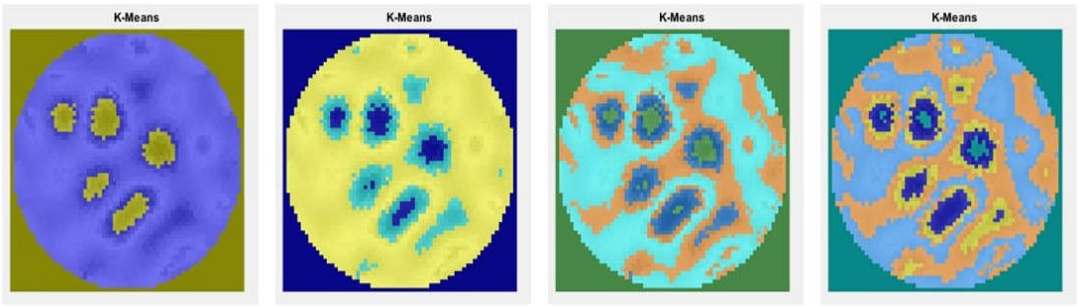

Figure 18 Segmentation module: Interactive observation of the K-means cluster regions (a) two clusters, (b) three clusters, (c) four clusters, and (d) five clusters.

5.3. Results for Sucrose crystallization using ERT-Vis

The results for the temperature from 90 °C until the 18 °C is presented in the Figure 19 (a-d). It can be observed that at 90 °C, the measurements give certain discontinuous region inside the reactor. These regions indicate the onset of crystallization over the electrodes. At 45 °C, some low conductivity regions are visible but the reconstructed images have significant noise. At 40 °C and 35 °C the sensors are completely blocked by the crystal formation over the electrodes and no electrical signal is able to pass through.

Preprints (www.preprints.org) | NOT PEER-REVIEWED | Posted: 6 May 2022 doi:10.20944/preprints202205.0072.v1

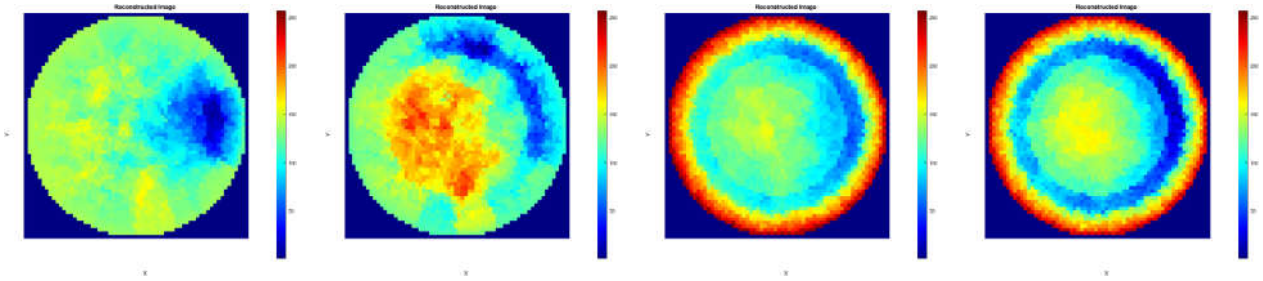

(a) (b) (c) (d)

Figure 19 Blocking of the sensor due to the sucrose crystallization over the ERT electrodes (a) 90 °C (b) 45 °C (c) 40 °C (d) 35 °C

6. Discussion

In this contribution, ERT-Vis a novel interactive application designed to facilitate Electrical Resistance Tomography (ERT) data visualization and evaluation was presented. ERT-Vis is an open-source MATLAB-based application software. The ERT-Vis software is versatile and extensible and it addresses a range of ERT process engineering and data visualization purposes. The primary contribution of ERT-Vis is that it enables rapid prototyping of different conductivity profiles acquired using an ERT device. This is useful when searching for the most efficient reconstruction-segmentation-visualization workflow for a new liquid media or a solid-liquid mixture.

The presented application case study involved domain experts and proved to be useful in determining the utility of the application for crystallization process monitoring. We envision numerous possibilities for data processing and implementation of control models and machine learning models using the refined ERT reconstructed image data. ERT-Vis would help researchers in streamlining the tasks at hand quickly and enable them to focus more on the analysis of the process data acquired. A tool facilitating obtaining a video file for the selected range of frames was also developed based on responses from the case study. We foresee implementing more EIDORS functions as well as analyses based on unsupervised learning into ERT-Vis. Such functionality will be offered as a user-friendly GUI for process applications. We also foresee keeping the software open source for further developments. This software has the potential to be further developed as a cloud-based service for industrial applications.

Supplementary Materials: The following are available online at www.mdpi.com/xxx/s1, Figure S1: title, Table S1: title, Video S1: title.

Author Contributions: Conceptualization, G.R., S.A., Y.Z., L.J.-S., M.F., and T.K.; methodology, G.R., S.A., Y.Z., M.F. and L.J.-S; software, G.R.; validation, G.R., S.A. and Y.Z.; formal analysis, G.R and S.A..; investigation, G.R., S.A., and Y.Z; resources, L.J.-S,T.K., and M. F.; data curation, G.R., Y.Z.; writing—original draft preparation, G.R., S. A., and Y.Z.; writing—review and editing, G.R., S.A., L.J.-S, Y.Z., T.K., and M. F.; visualization, G.R. and Y.Z.; supervision, T.K., L.J.-S. and M.F; project administration, G.R., T.K., L.J.-S., and M.F; All authors have read and agreed to the published version of the manuscript.

Funding: This project has received funding from the European Union's Horizon 2020 research and innovation programme under the Marie Sklodowska-Curie grant agreement No 764902.

Data Availability Statement: In this section, please provide details regarding where data supporting reported results can be found, including links to publicly archived datasets analyzed or generated during the study. Please refer to suggested Data Availability Statements in section "MDPI Research Data Policies" at https://www.mdpi.com/ethics. You might choose to exclude this statement if the study did not report any data.

Acknowledgments: The Author thanks Chalmer University of Technology for providing support during the secondment performed within TOMOCON project. The Author would like to thank LUT for providing the access to their chemical process laboratory. The Author would like to specially thank Prof. Laurent Babout from Lodz University of Technology for making all the project arrangements.

Conflicts of Interest: The authors declare no conflict of interest.

References

1. Larsen, P.A.; Patience, D.B.; Rawlings, J.B. Industrial Crystallization Process Control. *IEEE Control Systems Magazine* **2006**, *26*, 70–80.

2. Lewis, A.; Seckler, M.; Kramer, H.; Van Rosmalen, G. *Industrial Crystallization: Fundamentals and Applications*; Cambridge University Press, 2015;

3. Bowler, A.L.; Bakalis, S.; Watson, N.J. A Review of In-Line and on-Line Measurement Techniques to Monitor Industrial Mixing Processes. *Chemical Engineering Research and Design* **2020**, *153*, 463–495.

4. Scott, D.M. Recent Advances in In-Process Characterization of Suspensions and Slurries. *Powder Technology* **2022**, 117159.

5. Simon, L.L.; Simone, E.; Oucherif, K.A. Crystallization Process Monitoring and Control Using Process Analytical Technology. In *Computer Aided Chemical Engineering*; Elsevier, 2018; Vol. 41, pp. 215–242.

6. Myerson, A. *Handbook of Industrial Crystallization*; Butterworth-Heinemann, 2002; ISBN 0-08-053351-5.

7. Gao, Y.; Zhang, T.; Ma, Y.; Xue, F.; Gao, Z.; Hou, B.; Gong, J. Application of PAT-Based Feedback Control Approaches in Pharmaceutical Crystallization. *Crystals* **2021**, *11*, 221.

8. Lawrence, X.Y.; Lionberger, R.A.; Raw, A.S.; D'costa, R.; Wu, H.; Hussain, A.S. Applications of Process Analytical Technology to Crystallization Processes. *Advanced Drug Delivery Reviews* **2004**, *56*, 349–369.

9. Chianese, A.; Kramer, H.J. *Industrial Crystallization Process Monitoring and Control*; John Wiley & Sons, 2012; ISBN 3-527-64517-9.

10. Singh, M.R.; Chakraborty, J.; Nere, N.; Tung, H.-H.; Bordawekar, S.; Ramkrishna, D. Image-Analysis-Based Method for 3D Crystal Morphology Measurement and Polymorph Identification Using Confocal Microscopy. *Crystal growth & design* **2012**, *12*, 3735–3748.

11. Abu Bakar, M.; Nagy, Z.; Rielly, C. A Combined Approach of Differential Scanning Calorimetry and Hot-Stage Microscopy with Image Analysis in the Investigation of Sulfathiazole Polymorphism. *Journal of thermal analysis and calorimetry* **2010**, *99*, 609–619.

12. Simone, E.; Saleemi, A.N.; Nagy, Z.K. Raman, UV, NIR, and Mid-IR Spectroscopy with Focused Beam Reflectance Measurement in Monitoring Polymorphic Transformations. *Chemical Engineering & Technology* **2014**, *37*, 1305–1313.

13. Zhao, Y.; Wang, M.; Hammond, R.B. Characterization of Crystallisation Processes with Electrical Impedance Spectroscopy. *Nuclear engineering and design* **2011**, *241*, 1938–1944.

14. Eder, C.; Briesen, H. Impedance Spectroscopy as a Process Analytical Technology (PAT) Tool for Online Monitoring of Sucrose Crystallization. *Food Control* **2019**, *101*, 251–260.

15. Gherras, N.; Serris, E.; Févotte, G. Monitoring Industrial Pharmaceutical Crystallization Processes Using Acoustic Emission in Pure and Impure Media. *International Journal of pharmaceutics* **2012**, *439*, 109–119.

16. Ichitsubo, T.; Matsubara, E.; Kai, S.; Hirao, M. Ultrasound-Induced Crystallization around the Glass Transition Temperature for Pd40Ni40P20 Metallic Glass. *Acta materialia* **2004**, *52*, 423–429.

17. Prasad, R.; Dalvi, S.V. Sonocrystallization: Monitoring and Controlling Crystallization Using Ultrasound. *Chemical Engineering Science* **2020**, *226*, 115911.

18. Hampel, U.; Babout, L.; Banasiak, R.; Schleicher, E.; Soleimani, M.; Wondrak, T.; Vauhkonen, M.; Lähivaara, T.; Tan, C.; Hoyle, B. A Review on Fast Tomographic Imaging Techniques and Their Potential Application in Industrial Process Control. *Sensors* **2022**, *22*, 2309.

19. Merrifield, D.R.; Ramachandran, V.; Roberts, K.J.; Armour, W.; Axford, D.; Basham, M.; Connolley, T.; Evans, G.; McAuley, K.E.; Owen, R.L. A Novel Technique Combining High-Resolution Synchrotron x-Ray Microtomography and x-Ray Diffraction for Characterization of Micro Particulates. *Measurement Science and Technology* **2011**, *22*, 115703.

20. Polacci, M.; Arzilli, F.; La Spina, G.; Le Gall, N.; Cai, B.; Hartley, M.; Di Genova, D.; Vo, N.; Nonni, S.; Atwood, R. Crystallisation in Basaltic Magmas Revealed via in Situ 4D Synchrotron X-Ray Microtomography. *Scientific reports* **2018**, *8*, 1–13.

21. Koulountzios, P.; Aghajanian, S.; Rymarczyk, T.; Koiranen, T.; Soleimani, M. An Ultrasound Tomography Method for Monitoring CO2 Capture Process Involving Stirring and CaCO3 Precipitation. *Sensors* **2021**, *21*, 6995.

22. Wajman, R. The Concept of 3D ECT System with Increased Border Area Sensitivity for Crystallization Processes Diagnosis. *Sensor Review* **2021**.

23. McDonald, M.A.; Salami, H.; Harris, P.R.; Lagerman, C.E.; Yang, X.; Bommarius, A.S.; Grover, M.A.; Rousseau, R.W. Reactive Crystallization: A Review. *Reaction Chemistry & Engineering* **2021**, *6*, 364–400.

24. Karpiński, P.; Bałdyga, J. Precipitation Processes. *Handbook of Industrial Crystallization* **2019**, 216–265.

25. Rao, G.; Aghajanian, S.; Koiranen, T.; Wajman, R.; Jackowska-Strumiłło, L. Process Monitoring of Antisolvent Based Crystallization in Low Conductivity Solutions Using Electrical Impedance Spectroscopy and 2-D Electrical Resistance Tomography. *Applied Sciences* **2020**, *10*, 3903.

26. Rao, G.; Sattar, M.A.; Wajman, R.; Jackowska-Strumiłło, L. Quantitative Evaluations with 2d Electrical Resistance Tomography in the Low-Conductivity Solutions Using 3d-Printed Phantoms and Sucrose Crystal Agglomerate Assessments. *Sensors* **2021**, *21*, 564.

27. Aghajanian, S.; Rao, G.; Ruuskanen, V.; Wajman, R.; Jackowska-Strumillo, L.; Koiranen, T. Real-Time Fault Detection and Diagnosis of CaCO3 Reactive Crystallization Process by Electrical Resistance Tomography Measurements. *Sensors* **2021**, *21*, 6958.

28. Zhang, Y.; Fjeld, M.; Said, A.; Fratarcangeli, M. Task-Based Colormap Design Supporting Visual Comprehension in Process Tomography. In Proceedings of the EuroVis 2020 - Short Papers; Kerren, A., Garth, C., Marai, G.E., Eds.; The Eurographics Association, 2020.

29. Zhang, Y.; Fjeld, M.; Fratarcangeli, M.; Said, A.; Zhao, S. Affective Colormap Design for Accurate Visual Comprehension in Industrial Tomography. *Sensors* **2021**, *21*, 4766.

30. Hampel, U.; Wondrak, T.; Bieberle, M.; Lecrivain, G.; Schubert, M.; Eckert, K.; Reinecke, S. Smart Tomographic Sensors for Advanced Industrial Process Control TOMOCON. *Chemie Ingenieur Technik* **2018**, *90*, 1238–1239.

31. Liu, B.; Yang, B.; Xu, C.; Xia, J.; Dai, M.; Ji, Z.; You, F.; Dong, X.; Shi, X.; Fu, F. PyEIT: A Python Based Framework for Electrical Impedance Tomography. *SoftwareX* **2018**, *7*, 304–308, doi:https://doi.org/10.1016/j.softx.2018.09.005.

32. Grychtol, B.; Müller, B.; Adler, A. 3D EIT Image Reconstruction with GREIT. *Physiological measurement* **2016**, *37*, 785.

33. Wei, K.; Qiu, C.; Soleimani, M.; Primrose, K. ITS Reconstruction Tool-Suite: An Inverse Algorithm Package for Industrial Process Tomography. *Flow Measurement and Instrumentation* **2015**, *46*, 292–302, doi:https://doi.org/10.1016/j.flowmeasinst.2015.08.001.

34. Ye, L.; Yang, W. Real-Time 3D Visualisation in Electrical Capacitance Tomography. In Proceedings of the 2012 IEEE International Conference on Imaging Systems and Techniques Proceedings; IEEE, 2012; pp. 40–44.

35. Banasiak, R.; Jaworski, T.; Wajman, R. Aplikacja Dla Potrzeb Kompleksowego Przetwarzania Tomograficznych Danych Pomiarowych-TomoKIS Studio. *Zeszyty Naukowe Politechniki Lodzkiej* **2010**.

36. Vauhkonen, M.; Lionheart, W.R.; Heikkinen, L.M.; Vauhkonen, P.J.; Kaipio, J.P. A MATLAB Package for the EIDORS Project to Reconstruct Two-Dimensional EIT Images. *Physiological measurement* **2001**, *22*, 107.

37. Adler, A.; Lionheart, W.R. Uses and Abuses of EIDORS: An Extensible Software Base for EIT. *Physiological measurement* **2006**, *27*, S25.

38. Adler, A.; Lionheart, W.R.B. EIDORS: Towards a Community-Based Extensible Software Base for EIT. In Proceedings of the 6th Conf. on Biomedical Applications of Electrical Impedance Tomography; 2005; pp. 1–4.

 doi:10.20944/preprints202205.0072.v1

39. Lionheart, W.R.B.; Arridge, S.R.; Schweiger, M.; Vauhkonen, M.; Kaipio, J.P. Electrical Impedance and Diffuse Optical Tomography Reconstruction Software. In Proceedings of the Proceedings of 1st World Congress on Industrial Process Tomography; 1999; pp. 474–477.

40. Aghajanian, S.; Nieminen, H.; Laari, A.; Koiranen, T. Integration of a Calcium Carbonate Crystallization Process and Membrane Contactor–Based CO2 Capture. *Separation and Purification Technology* **2021**, 119043.

41. Honig, P. *Principles of Sugar Technology*; Elsevier, 2013;

42. Crestani, C.E.; Bernardo, A.; Costa, C.B.; Giulietti, M. Experimental Data and Estimation of Sucrose Solubility in Impure Solutions. *Journal of Food Engineering* **2018**, *218*, 14–23.

43. Jackson, R.F.; Silsbee, C.G. Saturation Relations in Mixtures of Sucrose, Dextrose, and Levulose. *Journal of the Franklin Institute* **1924**, *198*, 546–547.

44. Adler, A. *EIDORS Version 3.10*; DOI, 2019;

45. Polydorides, N.; Lionheart, W.R.B. A Matlab Toolkit for Three-Dimensional Electrical Impedance Tomography: A Contribution to the Electrical Impedance and Diffuse Optical Reconstruction Software Project. *Measurement science and technology* **2002**, *13*, 1871.

46. Campbell, R. *Mat2im*; 2020; https://www.mathworks.com/matlabcentral/fileexchange/26322-mat2im